Received: 14 September 2020 | Revised: 18 January 2021 | Accepted: 5 February 2021

DOI: 10.1002/mrm.28750

FULL PAPER

Magnetic Resonance in Medicine

Highly accelerated free-breathing real-time phase contrast cardiovascular MRI via complex-difference deep learning

Hassan Haji-Valizadeh[1] | **Rui Guo**[1] | **Selcuk Kucukseymen**[1] | **Amanda Paskavitz**[1] | **Xiaoying Cai**[1,2] | **Jennifer Rodriguez**[1] | **Patrick Pierce**[1] | **Beth Goddu**[1] | **Daniel Kim**[3] | **Warren Manning**[1,4] | **Reza Nezafat**[1]

[1]Department of Medicine (Cardiovascular Division), Beth Israel Deaconess Medical Center and Harvard Medical School, Boston, Massachusetts, USA

[2]Siemens Medical Solutions USA, Inc., Boston, Massachusetts, USA

[3]Department of Radiology, Northwestern University Feinberg School of Medicine, Chicago, Illinois, USA

[4]Department of Radiology, Beth Israel Deaconess Medical Center and Harvard Medical School, Boston, Massachusetts, USA

Correspondence
Reza Nezafat, Beth Israel Deaconess Medical Center, 330 Brookline Ave, Boston, MA 02215, USA.
Email: rnezafat@bidmc.harvard.edu

Funding information
Reza Nezafat receives grant funding by the NIH 5R01HL127015-02, 1R01HL129157-01A1, 5R01HL129185, and 1R01HL154744 (Bethesda, MD, USA); and the American Heart Association (AHA) 15EIA22710040 (Waltham, MA, USA). Dr. Haji-Valizadeh is supported by an NIH T32 training grant (5T32HL007374-41)

Purpose: To develop and evaluate a real-time phase contrast (PC) MRI protocol via complex-difference deep learning (DL) framework.

Methods: DL used two 3D U-nets to separately filter aliasing artifact from radial real-time velocity-compensated and complex-difference images. U-nets were trained with synthetic real-time PC generated from electrocardiograph (ECG) -gated, breath-hold, segmented PC (ECG-gated segmented PC) acquired at the ascending aorta of 510 patients. In 21 patients, free-breathing, ungated real-time (acceleration rate = 28.8) and ECG-gated segmented (acceleration rate = 2) PC were prospectively acquired at the ascending aorta. Hemodynamic parameters (cardiac output [CO], stroke volume [SV], and mean velocity at peak systole [peak mean velocity]) were measured for ECG-gated segmented and DL-filtered synthetic real-time PC and compared using Bland-Altman and linear regression analyses. Additionally, hemodynamic parameters were quantified from DL-filtered, compressed-sensing (CS) -reconstructed, and gridding reconstructed prospective real-time PC and compared to ECG-gated segmented PC.

Results: Synthetic real-time PC with DL showed strong correlation ($R > 0.98$) and good agreement with ECG-gated segmented PC for quantified hemodynamic parameters (mean-difference: CO = −0.3 L/min, SV = −4.3 mL, peak mean velocity = −2.3 cm/s). On average, DL required 0.39 s/frame to filter prospective real-time PC, which was 4.6-fold faster than CS. Compared to CS, DL showed superior correlation, tighter limits of agreement (LOAs), better bias for peak mean velocity, and worse bias for CO and SV. Compared to gridding, DL showed similar correlation, tighter LOAs for CO and SV, similar bias for CO, and worse bias for SV and peak mean velocity.

Conclusion: The complex-difference DL framework accelerated real-time PC-MRI by nearly 28-fold, enabling rapid free-running real-time assessment of flow hemodynamics.

KEYWORDS
compressed sensing, deep learning, GROG-GRASP, radial MRI, real-time phase contrast

1 | INTRODUCTION

Phase contrast (PC) MRI is routinely used in the clinic to measure blood flow in cardiovascular disease.[1-3] Typically, blood flow is evaluated using through-plane 2D PC MRI obtained with ECG gating and breath-holding to suppress cardiac and respiratory motion, respectively.[4] However, electrocardiograph (ECG)-gated, breath-hold PC MRI (ECG-gated segmented PC) is limited by the need for regular heart rhythm and adequate breath-hold capacity, which can result in image quality degradation in patients with dyspnea and/or arrhythmia. Additionally, breath-hold/gated imaging does not allow for "real-time" monitoring of blood flow changes with physiological provocation during exercise stress imaging.

Free-running real-time PC MRI enables heart rate insensitive imaging (ie, ungated) without the need for breath-holding or cardiac gating[5,6] but suffers from significant aliasing artifact due to the need for high MR acceleration. A number of strategies have been proposed to allow for real-time PC MRI, such as echo-planar imaging,[7] radial[8] k-space sampling, and spiral[9,10] k-space sampling combined with parallel imaging.[11,12] While promising, these methods often suffer from low spatial resolution ($>2.0 \times 2.0$ mm^2),[7-9] low temporal resolution (>50 ms),[7-10] and large slice thicknesses (>8 mm)[7,8,10] making clinical translation challenging. The combination of compressed sensing (CS)[13] with non-Cartesian sampling and parallel imaging[14,15] has been proposed as a solution to enable real-time PC with high spatial and temporal resolution. However, CS's clinical translation is limited by its lengthy image reconstruction time due to iterative optimization. For instance, on graphics processing unit (GPU) -equipped systems, CS requires 2.6 s/frame to reconstruct real-time PC acquired with radial k-space sampling[14] and 0.59 s/frames to reconstruct real-time PC acquired with spiral k-space sampling.[15]

Deep learning (DL) -based aliasing artifact removal in accelerated cardiovascular MRI has been proposed as an alternative to CS to reduce total reconstruction time[16-20] and improve performance.[19-21] Moreover, recent studies have shown the utility of DL-based methods for PC MRI. Vishnevskiy et al[21] showed that an unrolled network incorporating a physics-based model into the DL architecture reduces reconstruction time 30-fold compared to CS for 12.4- to 13.8-fold accelerated 4D ECG-gated segmented PC MRI with 25 cardiac phases. Ferdian et al[22] showed that 4DFlowNet network trained using synthetic 4D flow MR generated from computational fluid dynamic (CFD) solutions could be used to increase spatial resolution. Nath et al[23] showed that a U-net could filter aliasing artifact from accelerated (2.5-fold $\leq$ acceleration rate $\leq$ 5-fold) 2D PC MRI, while outperforming CS. While promising, DL is yet to be evaluated for de-aliasing real-time PC imaging.

In this study, we propose using a DL framework to remove aliasing artifact from highly accelerated (acceleration rate = 28.8) real-time PC images acquired with radial k-space sampling. The proposed framework consists of two DL modules that separately filter aliasing artifact from complex-difference and velocity-compensated images. The proposed DL method was trained using simulated radial k-space raw-data acquired at the ascending aorta in 510 patients undergoing clinical CMR exams using ECG-segmented PC with Cartesian sampling. We compared the performance of our proposed DL framework in 21 patients, who prospectively underwent both ungated free-breathing real-time PC and ECG-gated segmented PC at the ascending aorta. We demonstrated the robustness of the reconstruction under different conditions (ie, heavy breathing), imaging parameters, and anatomies in two additional healthy subjects.

2 | METHODS

2.1 | Subjects

This study was approved by the BIDMC Institutional Review Board (IRB) and was Health Insurance Portability and Accountability Act (HIPPA)-compliant. This study was performed under two IRB approved protocols, including one allowing use of retrospective data collected as part of a clinical exam for machine learning research; informed consent was waived for use of previously collected data. In addition, we prospectively recruited subjects for this study, and written-informed consent was obtained from all prospective participants. All MRI scans were conducted on a 3T scanner (MAGNETOM Vida, Siemens Healthcare, Erlangen, Germany) with body and spine phased-array coils (~30 elements).

For DL training, we used ECG-gated segmented PC k-space raw-data acquired at the ascending aorta in 510 patients (280 males, age = 55.8 ± 15.9 y), imaged between October 2018 and June 2019 during standard clinical workflow. For DL evaluation, an additional 21 patients (12 males, age = 56.7 ± 14.6 y) were prospectively recruited to undergo both ungated free-breathing real-time PC and ECG-gated segmented PC imaging. Furthermore, two healthy subjects (2 females, ages = 23 and 24 y) were prospectively

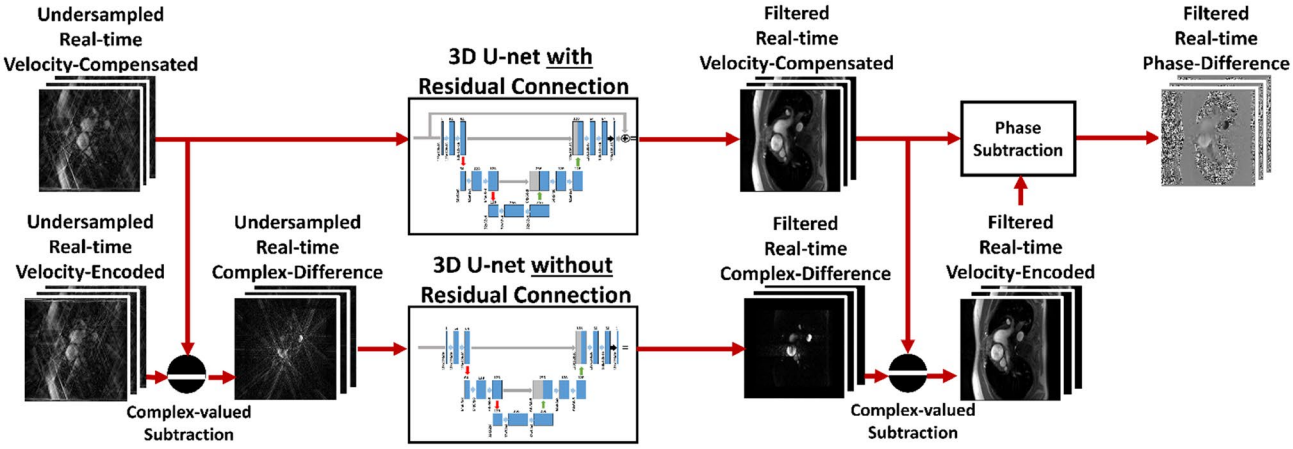

FIGURE 1 The proposed DL framework for real-time PC filtering. Undersampled complex-valued real-time velocity-compensated images and velocity-encoded images generated from raw k-space data were subtracted to produce undersampled real-time complex-difference images. Undersampled real-time velocity-compensated and complex-difference images were then filtered using two separate 3D U-net networks. Afterward, filtered real-time velocity-encoded images were calculated by subtracting filtered real-time complex-valued velocity-encoding and complex-difference images. Finally, filtered real-time phase-difference images were calculated by subtracting the phase information (phase subtraction) of filtered real-time velocity-compensated and velocity-encoded images

recruited to determine DL framework robustness in a pilot study. DL performance for different velocity sensitivity (V_{enc}) values (200-400 cm/s, step size = 50 cm/s) was assessed at the ascending aorta in one healthy subject. In the same subject, network performance for reconstructing real-time PC acquired with a V_{enc} of 300 cm/s at three different vessels (ie, pulmonic valve, right pulmonary artery, and left pulmonary artery) was evaluated. In another healthy volunteer, real-time PC was prospectively acquired during rest conditions and immediately after physiological exercise stress to assess the effect of heavy breathing and fast heart rate on quantified hemodynamic parameters. Exercise was performed with a supine bicycle ergometer (Lode B.V., Groningen, the Netherlands) secured onto the MRI table; such that, the subject exercised outside the magnet while on the table. Ergometer resistance was initially set to 0 watts and increased by steps of 15 watts every 2 min until reaching the target heart rate of 167 bpm.

2.2 | Pulse sequence

ECG-gated segmented PC used for network training and testing was acquired with two-fold accelerated Cartesian k-space sampling with parameters shown in Supporting Information Table S1. Accelerated ECG-gated segmented PC was reconstructed with generalized auto-calibrating partially parallel acquisitions (GRAPPA).[12] Residual background phase for ECG-gated segmented PC was corrected using standard methods[24] as follows: (1) Noisy voxels in the phase-difference image were removed with thresholding based on background noise SD; (2) Static tissue was isolated using a manually drawn region of interest (ROI); and (3) The background phase in the static tissue was fit to a first-order polynomial and then removed.

A real-time PC prototype sequence was implemented, as previously described,[14] using gradient-echo readout, radiofrequency (RF) spoiling, gradient spoiling, two-fold oversampling along the readout direction, and golden-angle radial k-space sampling[25] with an angular step of 111.25°. Velocity-compensated (V_{enc} = 0 cm/s) and velocity-encoded k-space lines were acquired in an interleaved manner with acquisition parameters presented in Supporting Information Table S1. Real-time PC images were reconstructed with five radial projections per frame which corresponded to a temporal resolution of 43.1 ms and an acceleration rate of 28.8. All real-time PC images were acquired with a dummy pre-scan (862 ms) used to drive magnetization to steady-state and to correct for trajectory errors.[14,26] Real-time PC background phase was corrected using the same procedure described for ECG-gated segmented PC, with the exception being that a second-order polynomial was used for static tissue phase fitting.[14]

2.3 | DL filtering framework

The proposed DL framework (Figure 1) filtered real-time PC as follows: undersampled real-time velocity-compensated and velocity-encoding images generated from raw k-space data were subtracted to produce undersampled real-time complex-difference images. Undersampled real-time velocity-compensated and complex-difference images were then filtered using two separate 3D U-nets.[19,27] Subsequently, filtered velocity-compensated and complex-difference images were subtracted to produce filtered velocity-encoded images. Finally, phase information of filtered velocity-compensated

and velocity-encoded images were subtracted to produce filtered real-time phase-difference images. The DL framework was implemented using PyTorch (Facebook, Menlo Park, California, USA). Both U-net architectures used for velocity-compensated and complex-difference filtering were composed of multi-scale decomposition of the input, skip connections, and convolutional layers composed of 3 × 3 × 3 convolutional kernel, batch normalization, and ReLu nonlinear thresh-holding (Figure 2). Real and imaginary components were concatenated to enable processing of complex datasets using a real DL network.[28] The only difference between the two 3D U-nets was an additional residual connection used for velocity-compensated image filtering that was not required for complex-difference filtering. We avoided using residual connection for complex-difference filtering in order to suppress output noise, which could have adversely affected hemodynamic quantification.

We designed our DL reconstruction framework to directly process hemodynamic velocity information by filtering complex-difference images. Typically, for PC MRI, phase-difference images are used to visualize and quantify important blood velocity information. However, phase-difference images present with significant salt-and-pepper noise in the image background, making direct DL processing challenging. Complex-difference imaging is an alternative strategy for isolating and visualizing hemodynamic information captured by PC MRI.[29] In complex-difference images, the image backgrounds present with near-zero signal intensity. Therefore, processing complex-difference images instead of phase-difference images can overcome the technical

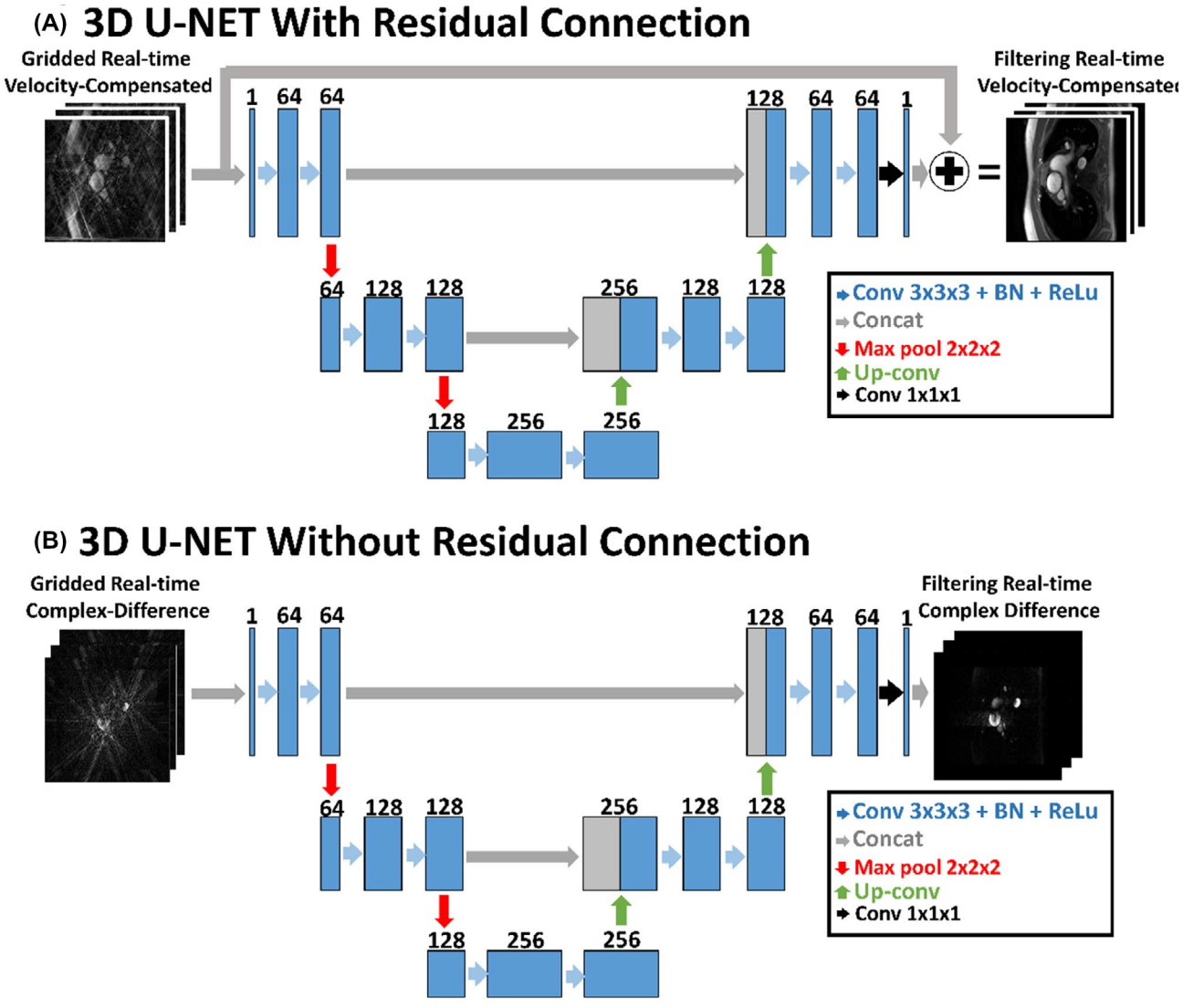

FIGURE 2 The two 3D U-net architectures used for DL filtering of real-time PC. Both 3D U-nets were composed of a set of 3 × 3 × 3 convolutional kernels with batch normalization and ReLU activation, 2 × 2 × 2 max pooling layers, 2 × 2 × 2 convolution transpose layers, and skip connections. One 3D U-net was used to filter velocity-compensated images (A), while the other was used to filter complex-difference images (B). The only difference between the two U-net architectures was an additional residual connection used for velocity-compensated filtering but not for complex-difference filtering

challenge associated with direct filtering of hemodynamic information.

2.4 | Generating training data for DL framework

For training of our DL model from ECG-gated PC MRI with Cartesian sampling, we simulated radial k-space sampling (Figure 3). The auto-calibration lines were used for GRAPPA[12] reconstruction of multi-coil ECG-gated segmented PC k-space raw-data (either velocity-compensated or velocity-encoded acquisitions). An offline GRAPPA reconstruction was implemented with code made available by Dr. Chiew (https://users.fmrib.ox.ac.uk/~mchiew/Teaching.html). GRAPPA-reconstructed multi-coil k-space was zero-filled to full size to compensate for asymmetric-echo acquisition. Multi-coil GRAPPA reconstructed images were cropped spatially to 128 × 128 matrix size and zero-filled to 168 × 168. Zero-filling was necessary to reduce artifact presentation in the outer region of the field of view (FOV). Auto-calibrated sensitivity profiles were derived from time-averaged multi-coil GRAPPA-reconstructed images.[30] Backward non-uniform fast Fourier transform

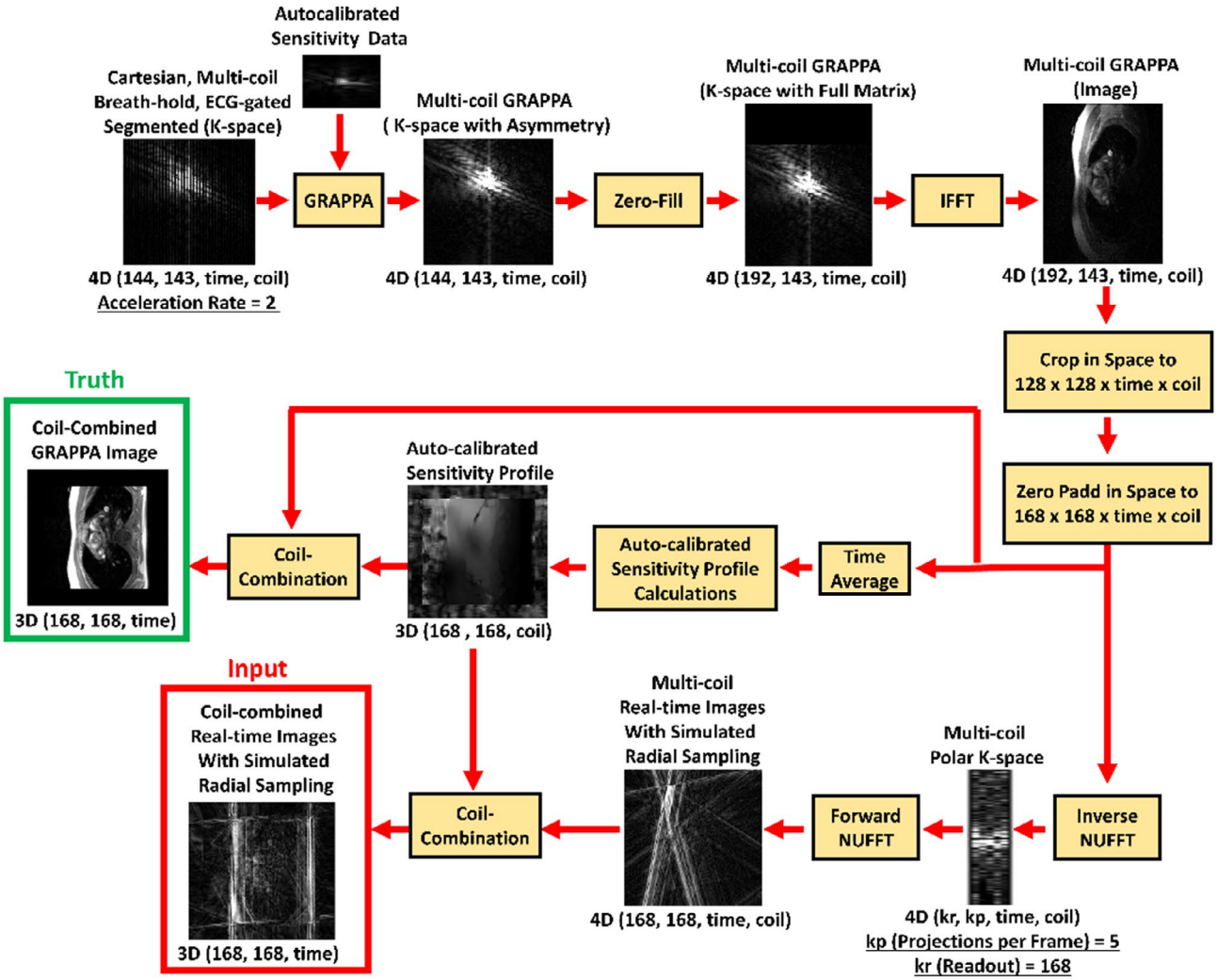

FIGURE 3 Procedure used to produce real-time velocity-compensated and velocity-encoded images with simulated radial k-space sampling. First, GRAPPA was used to reconstruct two-fold accelerated complex-valued, multi-coil k-space raw-data acquired during ECG-gated, segmented, breath-hold PC. Next, GRAPPA reconstructed k-space was zero-filled along the readout direction to compensate for asymmetric echo. Multi-coil GRAPPA-reconstructed images (produced using 2D IFFT operation) were spatially cropped to 128 × 128 matrix size and zero-padded to 168 × 168 matrix size. After zero-padding, multi-coil GRAPPA-reconstructed images were time averaged, and auto-calibrated sensitivity profiles were derived. Inverse NUFFT was then applied to spatially cropped multi-coil GRAPPA-reconstructed images to simulate multi-coil polar k-space acquisition with five radial projections per frame. Following backward NUFFT operation, forward NUFFT was applied to simulated polar data to produce multi-coil real-time images with simulated radial k-space sampling. Finally, both multi-coil GRAPPA reconstructions and corresponding multi-coil real-time images with simulated radial sampling were coil-combined using auto-calibrated sensitivity profiles. Real-time velocity-compensated and velocity-encoding images with simulated radial k-space sampling were produced separately

(NUFFT)[31] was applied to multi-coil GRAPPA reconstructions to simulate complex-valued polar data corresponding to golden-angle k-space radial sampling (five projections per frame). Following backward NUFFT operation, forward NUFFT was applied to simulated complex-valued polar data to produce real-time images with simulated radial sampling. Finally, both multi-coli, real-time images with simulated radial sampling and corresponding multi-coil GRAPPA-reconstructed images were coil-combined using auto-calibrated sensitivity profiles.[30] MATLAB (The MathWorks, Natick, MA) was used to execute all operations needed to simulate radial sampling, and the same procedure was used to produce real-time velocity-compensated and velocity-encoded images with simulated radial sampling. Real-time complex-difference images with simulated radial k-space sampling were produced through complex-valued subtraction of real-time velocity-compensated and velocity-encoded images with simulated radial sampling. Generated real-time PC datasets with simulated radial k-space sampling will be referred to as synthetic real-time PC throughout the manuscript.

2.5 | DL framework training

Both 3D U-net networks incorporated into the DL framework were separately trained to remove aliasing artifact from synthetic real-time complex-difference and velocity-compensated images. During each training iteration, U-nets received 16 (mini-batch size) different input/output dynamic series pairs (16 sequential temporal frames) composed of synthetic real-time images and corresponding coil-combined GRAPPA-reconstruction. Before training, both network input and output were centrally cropped to a size of 128 × 128 × 16. The number of temporal frames for ECG-gated segmented PC varied for each patient (16.2 ± 3.7 frames) based on heart rate. As such, for patients with ECG-gated segmented PC acquired with ≥16 temporal frames, the starting frame for the sequential dynamic series was randomly selected. For patients with ECG-gated segmented PC acquired with <16 temporal frames, the temporal sequence was circularly padded to 16 total frames. Velocity-compensated and velocity-encoded images from input (synthetic real-time) and output (GRAPPA reconstructions) pairs were scaled by the 95th percentile pixel intensity within the central 48 × 48 × 16 matrix corresponding to the magnitude of the velocity-compensated dataset. Scaling the velocity-encoded and velocity-compensated datasets by the same real-valued pixel intensity maintained phase-difference content, while scaling the complex-difference dataset by a real-valued constant. Training parameters were as follows: ADAM optimizer, 2900 iterations, learning rate = 0.001 (which decreased by 5% after every 100 iterations), 15% drop-out rate, and L_1 loss. Training of the velocity-compensated and complex-difference filtering networks took 6.1 and 6.5 h, respectively, using two of eight available GPUs on a NVIDIA (Santa Clara, California, USA) DGX-1 system equipped with 8T V100 GPUs (each having 32 GB memory and 5120 cores), CPU of 88 core: Intel Xeon 2.20GHZ each, and 504 GB RAM.

2.6 | Pre-processing for prospective real-time PC

Pre-processing to produce undersampled coil-combined real-time PC images (118 frames) for input into the DL filtering framework required the following steps: (1) Multi-coil real-time PC images were produced by gridding prospectively acquired multi-coil real-time PC polar k-space data using NUFFT; (2) Time-average gridded real-time PC images were then used to derive auto-calibrated sensitivity profiles[30]; (3) Coil-combined real-time PC images were produced by combining multi-coil real-time PC images with auto-calibrated sensitivity profiles; and (4) The real-time velocity-compensated and velocity-encoded images were scaled by the 95th percentile pixel intensity within the central 48 × 48 × 118 matrix of the velocity-compensated magnitude dataset, centrally cropped to a matrix size of 160 × 160 × 118, and then subtracted to generate complex-difference datasets (see Supporting Information Figure S1). Each prospective real-time PC dataset was fed individually into the DL filtering framework with all time frames acquired (118 frames) during ~5 s of scanning.

2.7 | CS reconstruction of real-time PC

GRAPPA operator gridding and golden-angle radial sparse parallel (GROG-GRASP) MRI reconstruction framework[32] was implemented in MATLAB for CS reconstruction of prospective real-time PC.[14] In short, multi-coil zero-filled Cartesian k-space data, auto-calibrated coil sensitivity profiles,[30] density-compensation matrix, and coil-combined zero-filled real-time images were derived during GROG-GRASP pre-processing. Auto-calibrated coil sensitivity profiles were produced using time averaged velocity-compensated dataset. Images were then fed into a nonlinear conjugate gradient optimization algorithm with back-tracking line search and temporal sparsity constraint to remove aliasing artifact. Velocity-compensated and velocity-encoded images were reconstructed separately using a normalized regularization weight of 0.0015 and 22 iterations. The optimal regularization weight was empirically determined through visual inspection of data fidelity, artifact suppression, and derived velocity profiles using one training dataset.[33] The gpuArray

functionality in MATLAB was used to reduce reconstruction time.

2.8 | Evaluation of DL for synthetic real-time PC

Synthetic real-time PC MRIs generated from ECG-gated segmented PC k-space raw-data corresponding to 21 test patients were filtered using the proposed DL framework. Using ECG-gated segmented PC as truth, normalized root mean squared error (NRMSE) and structural similarity index measure (SSIM) were calculated for real-time PC with and without DL filtering. Cardiac output (CO), stroke volume (SV), and mean velocity at peak systole (peak mean velocity) were quantified by one reader (H.H) who manually drew ROIs using in-house software in MATLAB for both synthetic real-time PC with DL and corresponding ECG-gated segmented PC. The same ROI was used to quantify hemodynamic parameters from ECG-gated segmented PC (truth) and DL-filtered synthetic real-time PC to avoid introducing error in hemodynamic measurements due to ROI size.

2.9 | Qualitative visual assessment of prospective real-time PC

Twenty-one sets (63 cases in total) of prospective real-time PC (with gridding, with DL, with CS) were randomized and de-identified. The ascending aorta edge definition for real-time PC was evaluated by an expert reader (S.K.) on a 3-point Likert scale as follows: 1 = non-diagnostic (cannot draw ROIs), 2 = diagnostic (adequate to draw ROIs), and 3 = excellent. Mean scores for real-time PC with gridding, CS, and DL were compared using Kruskal-Wallis test, followed by Dunn tests with Bonferroni correction for multiple comparisons between different groups. P-value < .05 was considered significant.

2.10 | Evaluation of DL-based de-aliasing of prospectively acquired real-time PC

Aliasing artifact in prospective real-time PC was filtered using DL and CS on the same workstation as previously described (DL Framework Training), except that a single GPU was used. The use of one GPU enabled fair comparison between both methods, as the implementation of the CS reconstruction on MATLAB allows for only one GPU. The total reconstruction time, calculated by adding pre-processing and de-aliasing times together, was recorded for each case reconstructed with gridding, CS, and DL. Pre-processing time was defined as the temporal duration required to produce undersampled coil-combined real-time PC images inputted into DL and CS. De-aliasing time referred to the temporal duration required by DL networks and CS iterative optimization to remove undersampling aliasing artifact.

ECG-gated segmented PC DICOMs (Digital Imaging and Communications in Medicine) were used as the gold-standard for DL and CS evaluation. ECG-gated segment PC DICOMs were reconstructed with a matrix of 192 × 192, FOV of 360 × 360 mm^2, interpolated temporal resolution of 28.6 to 43.6 ms, and 30 total time frames. CO, SV, and peak mean velocity were quantified by one reader (H.H.) for ECG-gated segmented PC and corresponding prospective real-time PC processed with gridding, CS, and DL. The same ROI (drawn on real-time PC with DL) was used for all real-time PC variants (ie, gridding, CS, DL) to avoid introducing error in hemodynamic measurements due to ROI size. In one healthy subject, the net volume and peak mean velocity was quantified for the pulmonic valve, left pulmonary artery, and right pulmonary artery. For prospective real-time PC, time curves associated with flow and mean velocity were extracted for every full heartbeat acquired (typically three to four heartbeats during 5 s acquisitions). Average CO, SV, and net flow were subsequently calculated from flow curves, and average peak mean velocity was calculated from mean velocity curves.

2.11 | Statistical analysis

A Kolmogorov-Smirnov test was performed to test the null hypothesis that all hemodynamic parameters quantified for 21 testing patients (CO, SV, peak mean velocity) were normally distributed at the 5% significance level. A paired t-test, Bland-Altman analysis, and linear-regression were used to compare hemodynamic parameters derived from ECG-gated segmented PC and synthetic real-time PC with DL. NRMSE and SSIM calculated for synthetic real-time PC with and without DL were compared using a paired t-test. For prospective real-time PC, one-way analysis of variance (ANOVA) with Bonferroni correction was used to compare hemodynamic parameters derived from all groups. Bland-Altman and linear-regression analyses were conducted on quantified hemodynamic parameters to determine levels of agreement and Pearson correlation (R) between ECG-gated segmented and real-time PC. A P-value < .05 was deemed significant for all statistical tests performed.

3 | RESULTS

Filtering complex-difference datasets instead of phase-difference images produced real-time PC with reduced artifacts (Supporting Information Figure S2, yellow and red

arrows). As shown in Supporting Information Figure S3, avoiding residual connection during DL filtering of real-time complex-difference images showed a noticeable reduction in artifact (red arrow). Figure 4A shows representative synthetic real-time complex-difference, velocity-compensated, and phase-difference images (drawn from the patient cohort used for network testing) with corresponding DL-filtered images and ECG-gated segmented PC. DL filtering significantly reduced aliasing artifact found in synthetic real-time PC images. For the same representative patient, Figure 4B shows flow and mean velocity curves quantified from synthetic real-time PC with DL (red) and truth (black). The proposed DL filtering framework improved ($P < .01$) the NRMSE and SSIM for both velocity-compensated (SSIM = 0.84 ± 0.05 vs. 0.17 ± 0.2, NRMSE = 2.2 ± 0.4% vs. 12.8 ± 2.1%) and complex-difference (SSIM = 0.80 ± 0.07 vs. 0.28 ± 0.05, NRMSE = 1.3 ± 0.4% vs. 4.9 ± 1.6%) synthetic datasets.

A Kolmogorov-Smirnov test showed that all hemodynamic parameters (CO, SV, peak mean velocity) quantified from ECG-gated segmented PC and synthetic real-time PC with DL were normally distributed ($P > .45$). According to the paired t-test, there were significant differences ($P < .01$) in CO, SV, and peak mean velocity between synthetic real-time PC with DL and ECG-gated segmented PC. As shown in Figure 5A, linear regression showed a strong Pearson correlation for ECG-gated segmented PC and synthetic real-time PC with DL for all categories (R ≥ 0.98). Bland-Altman analysis (Figure 5B) comparing synthetic real-time PC with DL and ECG-gated segmented PC (truth) showed the following results: CO (mean = 3.9 L/min; mean-difference = −0.3 L/min [−7.7% relative to mean], 95% limit of agreement (LOA) = −0.7 and 0.1 L/min), SV (mean = 55.4 mL; mean-difference = −4.3 mL [−7.8% relative to mean], 95% LOA = −9.8 and 1.1 mL), and peak mean velocity (mean = 50.7 cm/s; mean-difference = −2.3 cm/s [−4.5% relative to mean], 95% LOA = −8.5 to 4.0 cm/s).

Kruskal-Wallis test showed that DL (mean score = 2.7), CS (mean score = 2.0), and gridding (mean score = 1.0) produced ascending aorta edge sharpness which were significantly different ($P < .001$). Dunn tests showed significant differences ($P \leq .03$) for all combinations evaluated. CS and DL produced diagnostic (mean score ≥ 2.0) ascending aorta edge sharpness, and gridding produced non-diagnostic ascending aorta edge sharpness. Real-time PC (118 time-frames) with DL and CS required total reconstruction times of 46.5 ± 6.2 s (pre-processing = 40.9 ± 6.1 s; and de-aliasing = 5.6 ± 0.3 s) and 212.3 ± 48.9 s (pre-processing = 62.6 ± 14.6 s; and de-aliasing = 149.8 ± 34.6 s), respectively. As such, DL showed a 4.6-fold reduction in total reconstruction time and a 26.9-fold reduction in de-aliasing time compared to CS. For one representative patient, Figure 6 shows prospective real-time

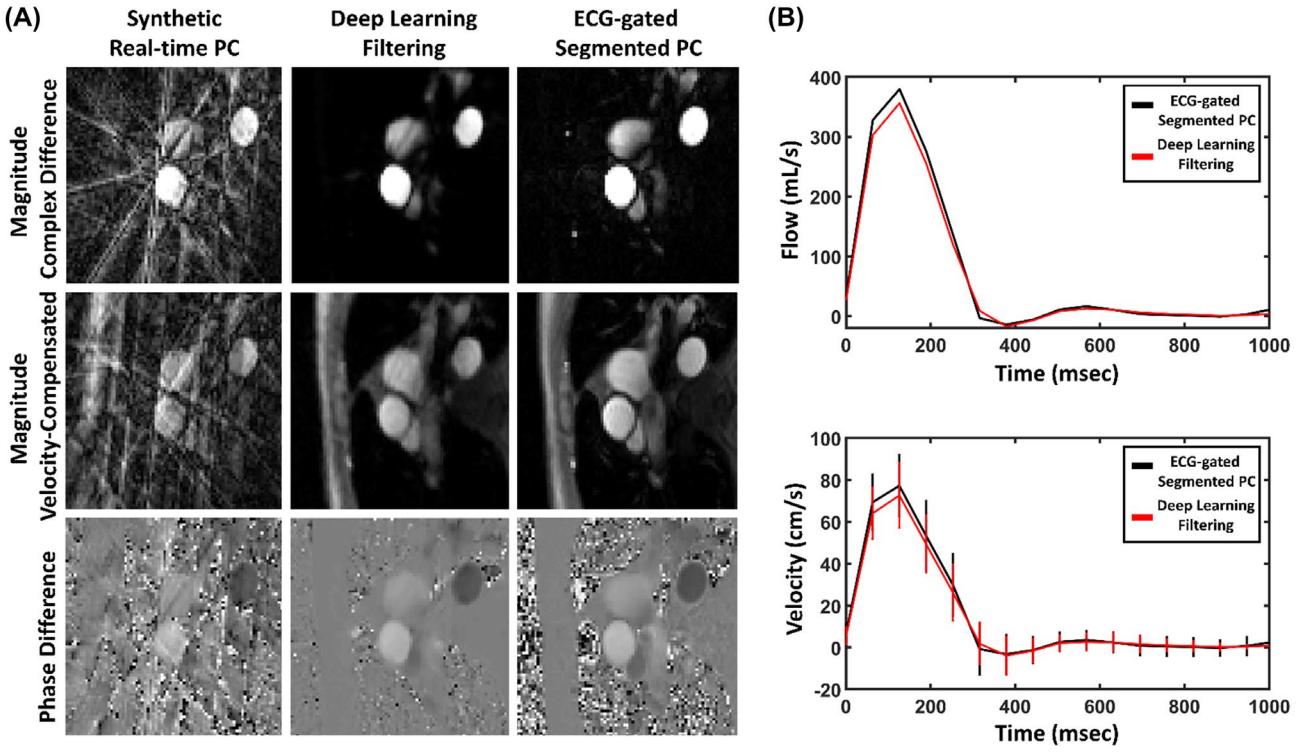

FIGURE 4 A, Synthetic real-time complex-difference, velocity-compensated, and phase-difference images (drawn from testing dataset), with their corresponding DL-filtered images and ECG-gated segmented PC. DL significantly reduces aliasing artifact present in the synthetic real-time PC. B, Flow and mean velocity curves generated from DL-filtered synthetic real-time PC (red) and ECG-gated segmented PC (black). Mean velocity curves are presented with error bars representing blood velocity SD within each time frame

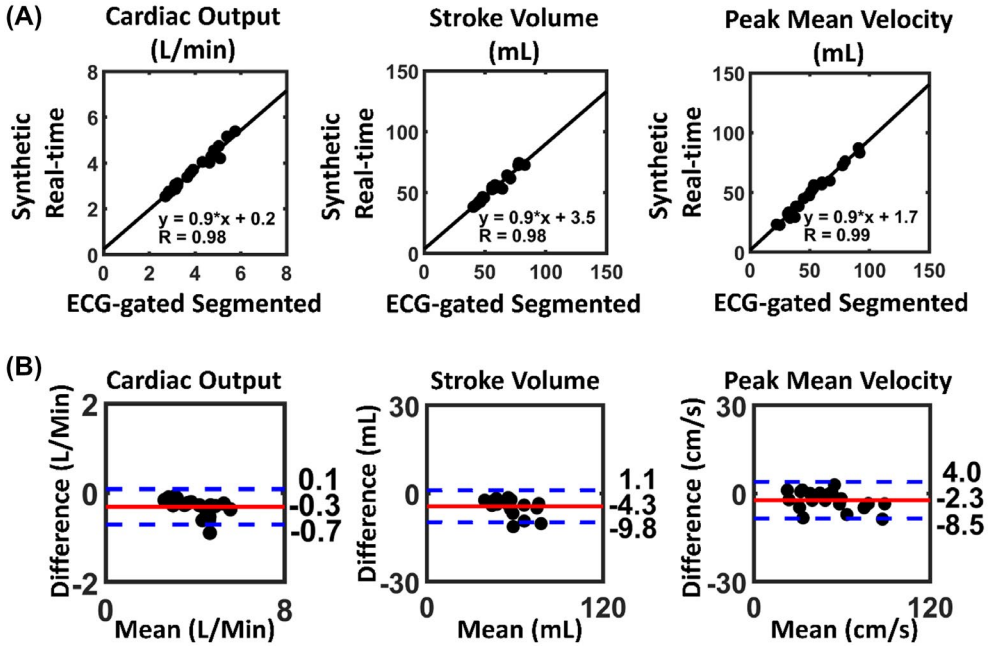

FIGURE 5 A, Linear regression results over all testing patients for synthetic real-time PC with DL-based filtering compared to ECG-gated segmented PC for derived CO, SV, and peak mean velocity. B, Bland-Altman plots for synthetic real-time PC with DL-based de-aliasing compared to ECG-gated segmented PC for CO, SV, and peak mean velocity. (Difference = synthetic real-time PC − ECG-gated segmented PC)

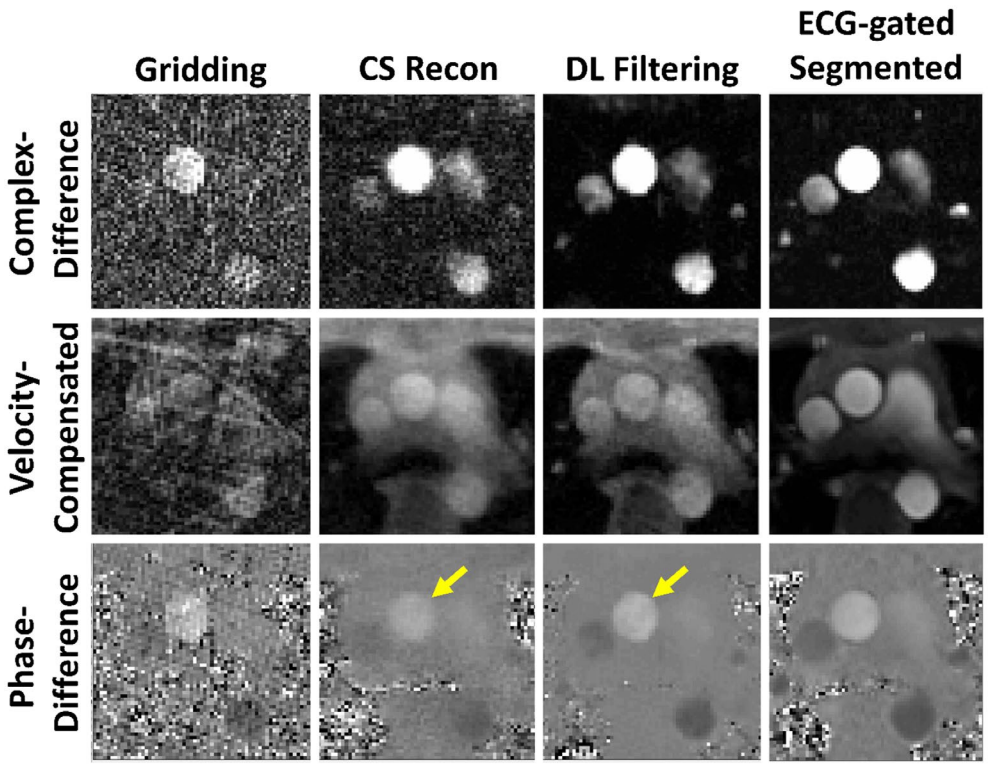

FIGURE 6 Real-time PC reconstructed with gridding, CS (CS recon), and filtered with DL (DL Filtering) and the corresponding ECG-gated segmented PC in one patient at end-systole. Compared to CS, DL filtering reduced imaging blurring at the ascending aorta (yellow arrow). The complete image series is provided in Supporting Information Video S1 for the real-time PC imaging and Supporting Information Video S2 for the ECG-gated segmented PC imaging

velocity-compensated, complex-difference, and phase-difference images after gridding, CS, and DL (Supporting Information Video S1) and their corresponding ECG-gated segmented PC (Supporting Information Video S2). For the same representative patient, Figure 7A shows flow and mean velocity curves quantified using real-time PC with DL filtering (red) and CS reconstruction (blue). For the same representative patient, Figure 7B shows flow and mean velocity time curves derived from composite heartbeats produced using real-time PC with DL (red) and CS (blue) and flow and mean velocity curves derived from ECG-gated segmented PC (black). Real-time flow and mean velocity time curves derived from composite heartbeats produced using DL (red) showed noticeably better agreement (ie, less underestimation at peak systole) than CS (blue) to ECG-gated segmented PC (black) (Figure 7B). Composite heartbeats were calculated by averaging the time curves quantified from each individual heartbeat acquired during real-time PC scanning.

For prospective real-time PC, a Kolmogorov-Smirnov test showed that all hemodynamic parameters quantified using DL-filtered real-time PC, CS reconstructed real-time PC, gridded real-time PC, and ECG-gated segmented PC were normally distributed ($P > .52$). According to one-way ANOVA analysis, there were no significant differences in quantified hemodynamic parameters ($P > .08$) for DL-filtered real-time PC, CS reconstructed real-time PC, gridded real-time PC, and ECG-gated segmented PC. Table 1 presents linear regression (Figure 8) and Bland-Altman (Figure 9) analysis results obtained from network testing using prospective real-time PC with DL, CS, and gridding.

Real-time PC prospectively acquired at the ascending aorta with different V_{enc} values produced phase-difference images of similar image quality with the following values: CO = 3.0 ± 0.1 L/min, SV = 41.2 ± 1.3 mL, and peak mean velocity = 63.7 ± 8.5 cm/s (Supporting Information Figure S4). DL successfully filtered prospective real-time PC imaging at three different vessels: pulmonic valve, left pulmonary artery, and right pulmonary artery (Supporting Information Figure S5). Real-time PC with DL at these vessels produced a net volume within 5 mL and a peak mean velocity within 2

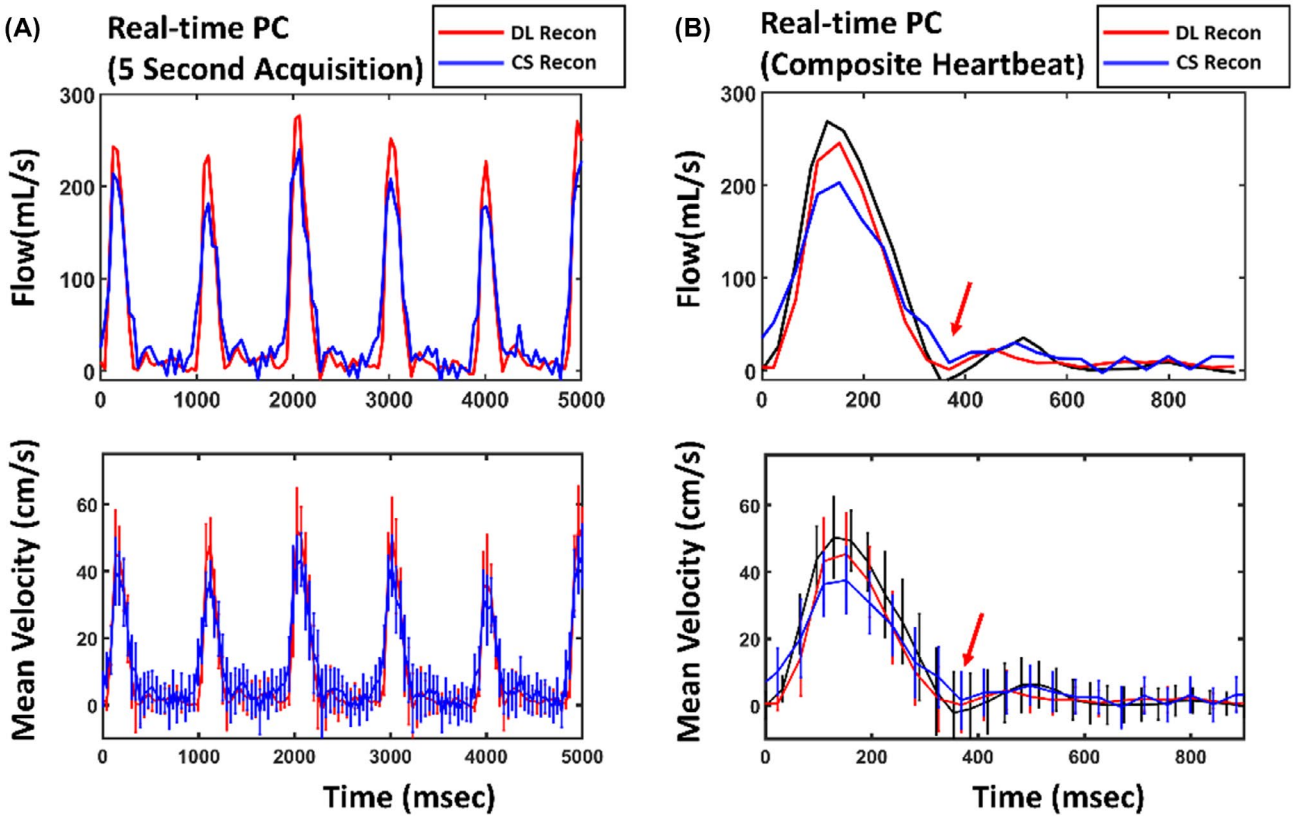

FIGURE 7 A, Real-time PC flow and mean velocity time curves acquired during 5 s of scanning in the datasets shown in Figure 6 and reconstructed with DL (red) and CS (blue). B, For the same patient, flow and mean velocity time curves quantified from ECG-gated segmented PC (black) and from a single composite heartbeat derived using DL-filtered (red) and CS- (blue) reconstructed real-time PC. Composite heartbeats were calculated by averaging flow and mean velocity time curves derived from each individual heartbeat obtained during 5 s real-time PC scanning. Flow and mean velocity time curves derived from composited heartbeats produced using DL-filtered real-time PC showed noticeably better agreement (ie, less underestimation at peak systole) than CS to ECG-gated segmented PC. As shown by the red arrow, both DL and CS were unable to capture backward blood flow with small magnitude. Note: mean velocity curves are presented with error bars representing the blood velocity standard deviation within each time frame

TABLE 1 Summary of linear regression and Bland-Altman analyses comparing ECG-gated segmented PC to prospectively acquired real-time PC with DL filtering, CS reconstruction, and gridding

Acquisition	Pearson correlation (R)	Mean difference	Mean	95% LOA (lower)	95% LOA (upper)
CO					
Real-time with DL vs. ECG-gated segmented	0.88	−0.8 L/min (−19.0% relative to mean)	4.2 L/min	−1.7 L/min	0.1 L/min
Real-time with CS vs. ECG-gated segmented	0.53	−0.3 L/min (−6.8% relative to mean)	4.4 L/min	−2.7 L/min	2.1 L/min
Real-time with gridding vs. ECG-gated segmented	0.87	−0.7 L/min (−16.7% relative to mean)	4.2 L/min	−1.8 L/min	0.4 L/min
SV					
Real-time with DL vs. ECG-gated segmented	0.87	−9.5 mL (−13.5% relative to mean)	70.4 mL	−24.2 mL	5.3 mL
Real-time with CS vs. ECG-gated segmented	0.65	−0.2 mL (−0.3% relative to mean)	75.1 mL	−41.0 mL	40.7 mL
Real-time with gridding vs. ECG-gated segmented	0.86	−7.6 (−10.7% relative to mean)	71.3 mL	−25.8 mL	10.5 mL
Peak Mean Velocity					
Real-time with DL vs. ECG-gated segmented	0.94	−4.4 cm/s (−8.4% relative to mean)	52.6 cm/s	−19.2 cm/s	10.4 cm/s
Real-time with CS vs. ECG-gated segmented	0.92	−10.3 cm/s (−20.8% relative to mean)	49.6 cm/s	−28.1 cm/s	8.0 cm/s
Real-time with gridding vs. ECG-gated segmented	0.93	2.4 cm/s (4.3% relative to mean)	56.0 cm/s	−13.1 cm/s	17.8 cm/s

cm/s to ECG-gated segmented PC (Supporting Information Table S2). Prospective real-time PC with DL detected a CO increase from a rest value of 4.9 L/min to an exercise stress value of 8.6 L/min (Supporting Information Figure S6).

4 | DISCUSSION

Our study describes the development of DL frameworks for reconstruction of free-breathing, ungated real-time PC. The proposed DL framework was composed of two 3D U-net networks trained with 510 synthetic real-time PC datasets and produced statistically significant improvements in NRMSE and SSIM for the synthetic real-time PC testing cohort. Hemodynamic parameters quantified for synthetic real-time PC in the testing cohort showed high correlation ($R \geq 0.98$) and good agreement (mean-differences: CO = −0.3 L/min, SV = −4.3 mL, and peak mean velocity = −2.3 cm/s). DL filtering of prospective real-time PC on average required 5.6 s (0.05 s/frame), which translated to a 26.9-fold reduction compared to CS. Total reconstruction time for DL (pre-processing and de-aliasing) on average required 46.5 s (0.39 s/frame), which translated to 4.6-fold reduction compared to CS. Compared to CS, prospective real-time PC with DL produced tighter LOA for CO and SV, better bias for peak mean velocity, and worse bias for CO and SV. Compared to gridding, prospective real-time PC with DL produced tighter LOA for CO and SV and worse bias for SV and peak mean velocity. DL was capable of filtering prospective real-time PC acquired with different V_{enc} values (100-400 cm/s) and at different vessels (pulmonic valve, right pulmonary artery, and left pulmonary artery). DL successfully filtered real-time PC at both rest and immediately after exercise stress.

Large and diverse high-quality training datasets are critical for DL network optimization. Hauptmann et al[19] proposed training DL using data derived from previously acquired DICOMs corresponding to clinical imaging in 250 pediatric patients. Using this strategy, Hauptmann et al showed that DL trained using synthetic real-time cine MRI could reconstruct radial real-time cine images five-fold faster than CS, while providing quantified functional parameters with superior agreement with ECG-gated, breath-hold cine MRI than CS. We adapted this approach to real-time PC reconstruction by training our DL framework using complex-valued, real-time PC training data with simulated radial k-space sampling derived from ECG-gated segmented PC k-space raw-data instead of DICOM images. Training with complex-valued k-space raw-data was necessary because the DICOM-making process strips critical phase information needed for PC reconstruction and therefore, is not optimal for real-time PC. To the best of our knowledge, this study is the first to explore the

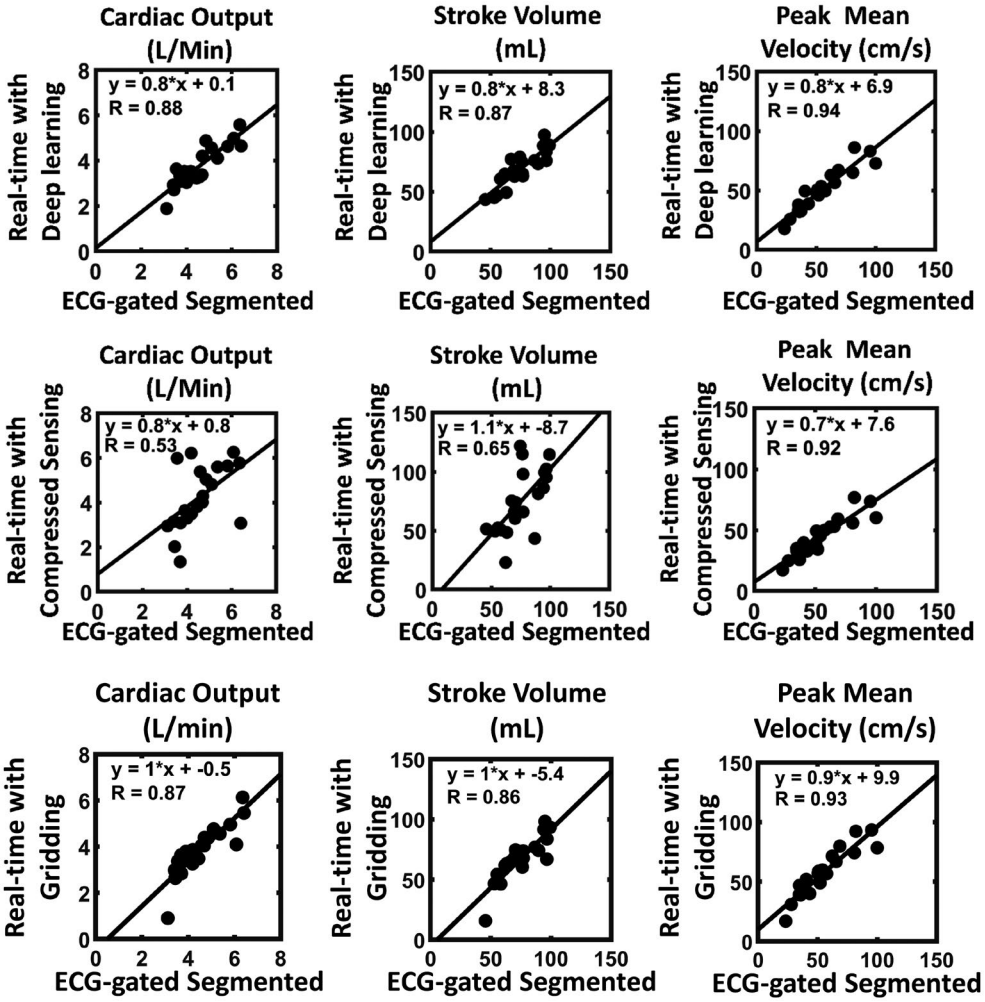

FIGURE 8 Linear regression results over all patients for real-time PC with DL filtering, CS reconstruction, and gridding reconstruction compared to ECG-gated segmented PC for derived CO, SV, and peak mean velocity. CO, SV, and peak mean velocities presented were calculated by averaging values over all full heartbeats scanned during real-time PC

efficacy of DL network training using synthetic real-time PC for the challenging task of real-time PC de-aliasing.

The work of Vishnevskiy et al[21] is a recent DL framework proposed for the reconstruction of accelerated PC MRI imaging. This study differs in the following ways: (1) U-net architectures were used for MR reconstruction instead of the physics-based model approach implemented by Vishnevskiy et al; (2) Significantly more training data were used in the present study (510 datasets obtained in patients vs. 11 datasets in healthy volunteers by Vishenevskiy et al); and (3) Vishenevskiy et al explored the use of DL for the reconstruction of 4D ECG-gated, breath-hold PC MRI prospectively acquired with Cartesian k-space sampling at an acceleration rate of approximately 14. In contrast, our study explored DL reconstruction of free-breathing and ungated 2D PC MRI acquired with radial k-space sampling at an acceleration rate of 28.8. A major clinical advantage of real-time PC is its natural resistance to image degradation caused by arrhythmia or dyspnea. Finally, Vishnevskiy et al proposed a DL network which did not directly process hemodynamic velocity information, but rather, reconstructed four velocity-encoded datasets. Our study showed that DL-based reconstruction of complex-difference images is a viable strategy for direct DL processing of hemodynamic velocity information. Previous work for CS[34,35] have shown the utility of using complex-difference processing to improve accelerated PC MRI reconstruction. However, to the best of our knowledge, we are the first group to show that complex-difference processing through DL can be used for filtering aliasing in accelerated PC MRI.

DL showed superior performance when evaluated using a testing data composed of synthetic real-time PC versus prospective real-time PC. Several reasons exist to explain DL's superior performance when evaluated with synthetic real-time PC. For instance, synthetic real-time PC was perfectly registered with truth, which was not the case for prospective real-time PC. Prospective real-time PC presented with higher order background phase compared to ECG-gated segmented PC used for training (first vs. second order). Differences

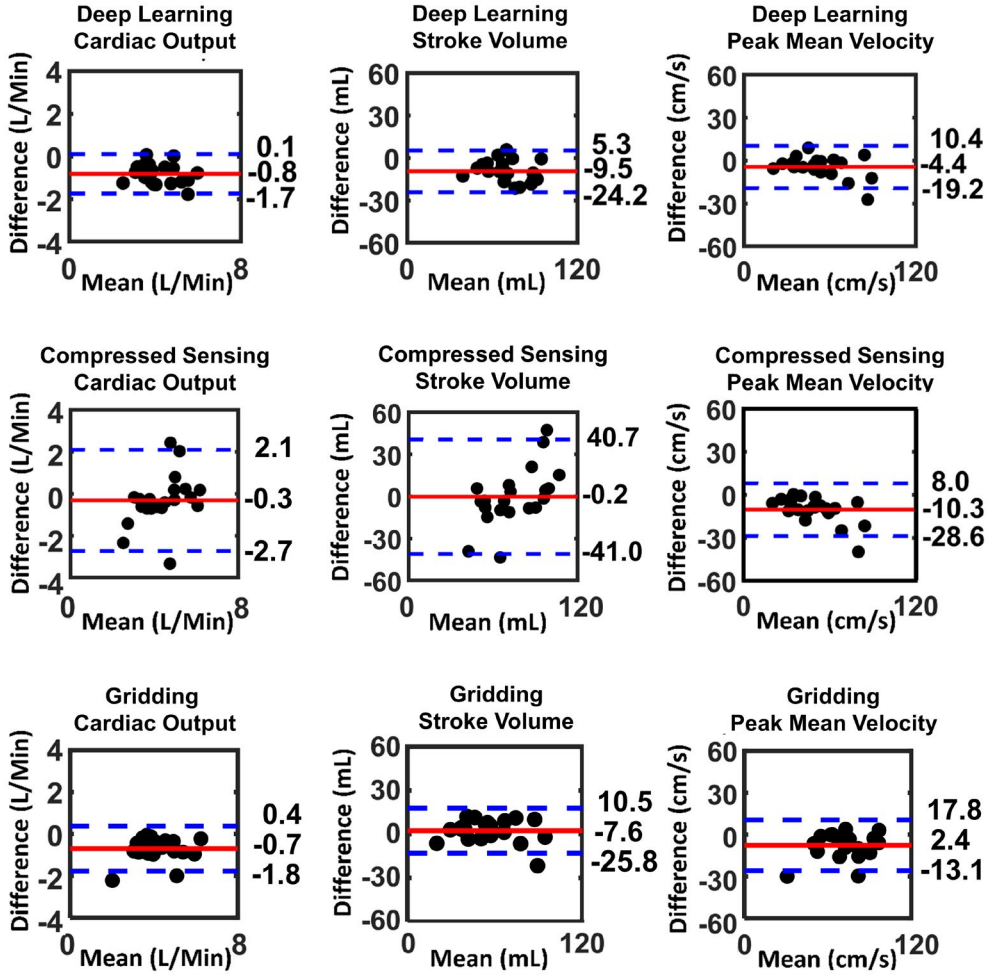

FIGURE 9 Bland-Altman plots for real-time PC with DL filtering, CS reconstruction, and gridding reconstruction compared to ECG-gated segmented PC for CO, SV, and peak mean velocity. CO, SV, and peak mean velocities presented were calculated by average values over all full heartbeats scanned during real-time PC. (Difference = real-time PC − ECG-gated segmented PC)

in background phase can be a potential source of error for DL filtering. Prospective real-time PC was acquired during free breathing; whereas, ECG-gated segmented PC used to generate synthetic real-time PC was acquired with cardiac gating during breath-holding. Differences in physiology (ie, intrathoracic pressure and heart rate variation) resulting from different breathing states may lead to error when comparing prospective real-time and ECG-gated segmented PC. Furthermore, the DL network was not able to learn breathing motion expected for prospective real-time PC because the training datasets were generated from breath-hold ECG-gated PC.

Our study has several limitations. This study did not explore the capacity of DL-filtered real-time PC to evaluate the effect of beat-to-beat variations on hemodynamics. Instead, average CO, SV, and peak mean velocity over multiple heartbeats were calculated. All DL-filtered and CS reconstructions were performed offline. Additional work is required to incorporate the proposed DL framework into vendor-provided inline image reconstruction pipelines. The DL framework was compared solely to CS and not to alternative reconstruction methods for radial real-time PC, such as non-linear inversion (NLINV)[5,6,26,36] reconstruction. For DL training, the input and truth for velocity-compensated and velocity-encoded datasets were scaled separately, which can be a potential source of error. Real and imaginary components of complex-valued velocity-compensated and complex-difference datasets were concatenated to enable DL processing with real-valued convolutional kernels. Alternatively, complex-valued convolutional kernels[16] may be used, but such an approach requires a two-fold increase in the number of convolutional kernel parameters and a four-fold increase in the number of operations. Prospective real-time PC was obtained with V_{enc} of 300 cm/s to match our clinical practice. Our clinical practice uses a single 300 cm/s V_{enc} for all ascending aorta imaging regardless of individual patient characteristics. This approach avoids the need for V_{enc} scouts but can result in increased phase noise. Image quality was assessed for only real-time PC variants (ie, gridding, CS, and DL). Additional studies comparing the image quality of real-time PC with DL to

ECG-gated segmented PC are needed to determine if real-time PC with DL is a viable alternative. When analyzed using the same ROIs, real-time PC with gridding produced similar correlation as DL to ECG-gated segmented PC (CO = 0.88 vs. 0.87, SV = 0.87 vs. 0.86, peak mean velocity = 0.94 vs. 0.93) and superior bias than DL for SV (−9.5 vs. −7.6 L/min) and peak mean velocity (−4.4 vs. 2.4 cm/s). Expecting such a performance in the clinic is unrealistic given that ROIs cannot be directly drawn on real-time PC with gridding because of non-diagnostic ascending aorta edge definition (mean score = 1). Approximately 40 s were needed to reconstruct accelerated real-time PC using an off-line workstation after k-space acquisition was completed. Alternatively, real-time PC can be deployed to produce a "real-time" stream of images by reconstructing a smaller subset of frames (~ five frames) during k-space acquisition. Such a strategy will require the re-training of the DL network with five-time frames and would require additional effort to integrate the proposed DL pipeline into a vendor inline reconstruction platform. The proposed DL framework required complicated methodology to generate training data. A simulated training data approach (ie, CFD generated flow profiles) as used by Ferdian et al[22] may serve as a simpler alternative for generating DL training data. Despite our best efforts, a large portion of the total reconstruction time for CS and DL was due to pre-processing time [DL = 40.9 s (88.0% of total recon time), CS = 62.6 s (30.0 % of total recon time)]. A future study focused on reducing pre-processing time through faster gridding implementations such as Trajectory-optimized NUFFT (TRON)[37] is desirable. For this proof-of-concept study, we did not evaluate DL performance in patients with suspected aortic valve disease. Further studies are required to assess the diagnostic performance of the proposed DL framework in this patient cohort.

In conclusion, the proposed DL framework enables rapid reconstruction of highly accelerated (acceleration rate = 28.8) ungated free-breathing real-time PC using synthetic real-time PC as training data and two 3D U-nets to separately filter velocity-compensated and complex-difference images. Furthermore, the proposed DL framework enabled 4.6-fold faster real-time PC reconstruction compared to CS.

ACKNOWLEDGMENTS

Dr. Hassan Haji-Valizadeh is currently an employee of Canon Medical Research USA Inc. The work presented in this study was performed during his post-doctoral training fellowship at Beth Israel Deaconess Medical Center.

CONFLICT OF INTEREST

Dr. Nezafat, one of the co-authors of this work, has a research agreement with Siemens Medical Solutions USA, Inc, the manufacturer of the MRI system used in this study. Dr. Cai, one of the co-authors of this work, is an employee of Siemens Medical Solutions USA, Inc.

DATA AVAILABILITY STATEMENT

Deep learning and compressed sensing reconstruction codes used are available on Harvard dataverse (https://dataverse.harvard.edu/dataverse/cardiacmr), reference number (doi.org/10.7910/DVN/N97M6H).

ORCID

Hassan Haji-Valizadeh https://orcid.org/0000-0002-7652-1748
Rui Guo https://orcid.org/0000-0002-5188-6281
Selcuk Kucukseymen https://orcid.org/0000-0002-9757-3088
Daniel Kim https://orcid.org/0000-0003-2660-8973

REFERENCES

1. Pelc NJ, Herfkens RJ, Shimakawa A, Enzmann DR. Phase contrast cine magnetic resonance imaging. *Magn Reson Q*. 1991;7:229-254.
2. Rebergen SA, van der Wall EE, Doornbos J, de Roos A. Magnetic resonance measurement of velocity and flow: technique, validation, and cardiovascular applications. *Am Heart J*. 1993;126:1439-1456.
3. Nayler GL, Firmin DN, Longmore DB. Blood flow imaging by cine magnetic resonance. *J Comput Assist Tomogr*. 1986;10:715-722.
4. Gatehouse PD, Keegan J, Crowe LA, et al. Applications of phase-contrast flow and velocity imaging in cardiovascular MRI. *Eur Radiol*. 2005;15:2172-2184.
5. Joseph A, Kowallick JT, Merboldt K-D, et al. Real-time flow MRI of the aorta at a resolution of 40 msec. *J Magn Reson Imaging*. 2014;40:206-213.
6. Joseph AA, Merboldt K-D, Voit D, et al. Real-time phase-contrast MRI of cardiovascular blood flow using undersampled radial fast low-angle shot and nonlinear inverse reconstruction. *NMR Biomed*. 2012;25:917-924.
7. Lin H-Y, Bender JA, Ding YU, et al. Shared velocity encoding: a method to improve the temporal resolution of phase-contrast velocity measurements. *Magn Reson Med*. 2012;68:703-710.
8. Shankaranarayanan A, Simonetti OP, Laub G, Lewin JS, Duerk JL. Segmented k-space and real-time cardiac cine MR imaging with radial trajectories. *Radiology*. 2001;221:827-836.
9. Nayak KS, Pauly JM, Kerr AB, Hu BS, Nishimura DG. Real-time color flow MRI. *Magn Reson Med*. 2000;43:251-258.
10. Nezafat R, Kellman P, Derbyshire JA, McVeigh ER. Real-time blood flow imaging using autocalibrated spiral sensitivity encoding. *Magn Reson Med*. 2005;54:1557-1561.
11. Pruessmann KP, Weiger M, Scheidegger MB, Boesiger P. SENSE: sensitivity encoding for fast MRI. *Magn Reson Med*. 1999;42:952-962.
12. Griswold MA, Jakob PM, Heidemann RM, et al. Generalized autocalibrating partially parallel acquisitions (GRAPPA). *Magn Reson Med*. 2002;47:1202-1210.
13. Lustig M, Donoho D, Pauly JM. Sparse MRI: the application of compressed sensing for rapid MR imaging. *Magn Reson Med*. 2007;58:1182-1195.
14. Haji-Valizadeh H, Feng L, Ma LE, et al. Highly accelerated, real-time phase-contrast MRI using radial k -space sampling and GROG-GRASP reconstruction: a feasibility study in pediatric patients

with congenital heart disease. *NMR Biomed*. 2020;33:e4240. http://dx.doi.org/10.1002/nbm.4240.
15. Kowalik GT, Knight D, Steeden JA, Muthurangu V. Perturbed spiral real-time phase-contrast MR with compressive sensing reconstruction for assessment of flow in children. *Magn Reson Med*. 2020;83:2077-2091.
16. El-Rewaidy H, Neisius U, Mancio J, et al. Deep complex convolutional network for fast reconstruction of 3D late gadolinium enhancement cardiac MRI. *NMR Biomed*. 2020;33:1195-1208. https://www.ncbi.nlm.nih.gov/pubmed/32352197
17. Fan L, Shen D, Haji-Valizadeh H, et al. Rapid dealiasing of undersampled, non-Cartesian cardiac perfusion images using U-net. *NMR Biomed*. 2020;33:e4239. http://dx.doi.org/10.1002/nbm.4239.
18. Haji-Valizadeh H, Shen D, Avery RJ, et al. Rapid reconstruction of Four-dimensional MR angiography of the thoracic aorta using a convolutional Neural Network. *Radiol Cardiothorac Imaging*. 2020;2:e190205. http://dx.doi.org/10.1148/ryct.2020190205.
19. Hauptmann A, Arridge S, Lucka F, Muthurangu V, Steeden JA. Real-time cardiovascular MR with spatio-temporal artifact suppression using deep learning-proof of concept in congenital heart disease. *Magn Reson Med*. 2019;81:1143-1156.
20. Schlemper J, Caballero J, Hajnal JV, Price AN, Rueckert D. A deep cascade of convolutional neural networks for dynamic MR image reconstruction. *IEEE Trans Med Imaging*. 2018;37:491-503.
21. Vishnevskiy V, Walheim J, Kozerke S. Deep variational network for rapid 4D flow MRI reconstruction. *Nat Mach Intell*. 2020;2:228-235.
22. Ferdian E, Suinesiaputra A, Dubowitz DJ, et al. 4DFlowNet: super-resolution 4D flow MRI using deep learning and computational fluid dynamics. *Front Phys*. 2020;8:138. http://dx.doi.org/10.3389/fphy.2020.00138.
23. Nath R, Callahan S, Singam N, Stoddard M, Amini AA. Accelerated phase contrast magnetic resonance imaging via deep learning. Paper presented at: 2020 IEEE 17th International Symposium on Biomedical Imaging (ISBI); 2020; Iowa City, IA, USA.
24. Stalder AF, Russe MF, Frydrychowicz A, Bock J, Hennig J, Markl M. Quantitative 2D and 3D phase contrast MRI: optimized analysis of blood flow and vessel wall parameters. *Magn Reson Med*. 2008;60:1218-1231.
25. Winkelmann S, Schaeffter T, Koehler T, Eggers H, Doessel O. An optimal radial profile order based on the golden ratio for time-resolved MRI. *IEEE Trans Med Imaging*. 2007;26:68-76.
26. Untenberger M, Tan Z, Voit D, et al. Advances in real-time phase-contrast flow MRI using asymmetric radial gradient echoes. *Magn Reson Med*. 2016;75:1901-1908.
27. Han Y, Yoo J, Kim HH, Shin HJ, Sung K, Ye JC. Deep learning with domain adaptation for accelerated projection-reconstruction MR. *Magn Reson Med*. 2018;80:1189-1205.
28. Eo T, Jun Y, Kim T, Jang J, Lee HJ, Hwang D. KIKI-net: cross-domain convolutional neural networks for reconstructing undersampled magnetic resonance images. *Magn Reson Med*. 2018;80:2188-2201.
29. Bernstein MA, Ikezaki Y. Comparison of phase-difference and complex-difference processing in phase-contrast MR angiography. *J Magn Reson Imaging*. 1991;1:725-729.
30. Walsh DO, Gmitro AF, Marcellin MW. Adaptive reconstruction of phased array MR imagery. *Magn Reson Med*. 2000;43:682-690.
31. Matej S, Fessler JA, Kazantsev IG. Iterative tomographic image reconstruction using Fourier-based forward and back-projectors. *IEEE Trans Med Imaging*. 2004;23:401-412.
32. Benkert T, Tian Y, Huang C, DiBella EVR, Chandarana H, Feng L. Optimization and validation of accelerated golden-angle radial sparse MRI reconstruction with self-calibrating GRAPPA operator gridding. *Magn Reson Med*. 2018;80:286-293.
33. Haji-Valizadeh H, Collins JD, Aouad PJ, et al. Accelerated, free-breathing, noncontrast, electrocardiograph-triggered, thoracic MR angiography with stack-of-stars k-space sampling and GRASP reconstruction. *Magn Reson Med*. 2019;81:524-532.
34. Kwak Y, Nam S, Akçakaya M, et al. Accelerated aortic flow assessment with compressed sensing with and without use of the sparsity of the complex difference image. *Magn Reson Med*. 2013;70:851-858.
35. Sun A, Zhao BO, Ma KE, et al. Accelerated phase contrast flow imaging with direct complex difference reconstruction. *Magn Reson Med*. 2017;77:1036-1048.
36. Tan Z, Roeloffs V, Voit D, et al. Model-based reconstruction for real-time phase-contrast flow MRI: improved spatiotemporal accuracy. *Magn Reson Med*. 2017;77:1082-1093.
37. Smith DS, Sengupta S, Smith SA, Brian WE. Trajectory optimized NUFFT: Faster non-Cartesian MRI reconstruction through prior knowledge and parallel architectures. *Magn Reson Med*. 2019;81:2064-2071.

SUPPORTING INFORMATION

Additional supporting information may be found online in the Supporting Information section.

FIGURE S1 DL filtering framework including preparation and post-processing steps. Real-time velocity-compensated and velocity-encoded images were scaled by the 95th percentile pixel intensity within the central $48 \times 48 \times 118$ matrix corresponding to the magnitude of the velocity-compensated dataset. Afterwards, both velocity-compensated and velocity-encoded images were centrally cropped to a size of $160 \times 160 \times 118$, and real and imaginary components were concatenated. Real-time complex-difference datasets were produced by subtracting velocity-compensated datasets and velocity-encoded. Real-time complex-difference and velocity-compensated datasets were inputted into 3D U-nets with all 118 time frames. Filtered velocity-encoding dataset was produced by subtracting DL filtered complex-difference datasets from velocity-compensated. Filtered phase-difference datasets were derived from the phase subtraction of filtered velocity-encoded and velocity-compensated dataset

FIGURE S2 Representative synthetic real-time phase-difference images with simulated radial k-space sampling (drawn from our training dataset), direct deep learning (DL) filtering of phase-difference images, DL filtering of complex-difference images (proposed method), and their corresponding ECG-gated segmented phase-difference images. Phase-difference images produced through direct DL filtering

present with more artifact at the ascending (yellow arrow) and descending (red arrow) aortas than phase-difference images produced through DL de-aliasing of complex-difference images. Observed reduction in image quality may be due to the presence of salt-and-pepper noise found in the phase-difference background (blue circle)

FIGURE S3 Synthetic real-time complex-difference and velocity-compensated images at systole and diastole for the following conditions: after U-net filtering without residual connection, after U-net filtering with residual connection, and ECG-gated segmented PC (truth). As demonstrated, incorporating the residual connection into the U-net architecture resulted in increased residual artifact (red arrow) and increased noise in the ascending aorta (yellow arrow). No difference was observed for velocity-compensated dataset de-aliased using U-net with and without residual connection

FIGURE S4 Prospective real-time PC datasets acquired at the ascending aorta of a single healthy volunteer with different V_{enc} values. As shown, real-time PC acquired with different V_{enc} values at the same image orientation produced similar image quality after DL filtering

FIGURE S5 Prospective real-time PC datasets with DL filtering and ECG-gated segmented PC images acquired at three different vessels (ie, pulmonic valve, left pulmonary artery, right pulmonary artery) and corresponding mean velocity time curves (composite heart-beat) for a single healthy volunteer. Mean velocity curves are presented with error bars representing blood velocity standard-deviation at each time point

FIGURE S6 Prospective real-time PC datasets with DL filtering and corresponding mean velocity time curves obtained in one single healthy volunteer during rest and immediately after exercise stress. Real-time PC acquired immediately after exercise produced a much higher cardiac output (8.6 L/min) than real-time PC acquired during rest (4.9 L/min). Mean velocity curves are presented with error bars representing blood velocity standard deviation at each time frame

TABLE S1 Summary of acquisition parameters for ECG-gated segmented PC used for network training and testing, and prospective real-time PC used for network testing

TABLE S2 Summary of expert reader scores for the ascending aorta edge sharpness for prospective real-time PC after gridding alone, compressed sensing (CS) reconstruction, and after deep learning (DL) filtering. Reported values represent mean (range min:max)

TABLE S3 Net volume and peak mean velocity quantified at the pulmonic valve, left pulmonary artery, and right pulmonary artery for one healthy volunteer who underwent both ECG-gated segmented PC and prospective real-time PC acquisition

VIDEO S1 Movie display of prospectively acquired real-time complex-difference (row 1), velocity-compensated (row 2), and phase-difference (row 3) images reconstructed with gridding (column 1), compressed sensing (column 2), and deep learning (column 3) for one representative patient shown in Figure 6

VIDEO S2 Movie display of breath-hold, ECG-gated, segmented complex-difference (column 1), velocity-compensated (column 2), and phase-difference (column 3) images from one representative patient shown in Figure 6

How to cite this article: Haji-Valizadeh H, Guo R, Kucukseymen S, et al. Highly accelerated free-breathing real-time phase contrast cardiovascular MRI via complex-difference deep learning. *Magn Reson Med*. 2021;86:804–819. https://doi.org/10.1002/mrm.28750